Ion Current Density Profile of an Erosion Free Low Power Hall Thruster

IEPC-2017-436

Presented at the 35th International Electric Propulsion Conference
Georgia Institute of Technology • Atlanta, Georgia • USA
October 8 – 12, 2017

Burak Karadag[1]
The Graduate University for Advanced Studies (SOKENDAI), Japan

Shinatora Cho[2] and Ikkoh Funaki[3]
Japan Aerospace Exploration Agency

Abstract: In our previous paper, we introduced external discharge plasma thruster (XPT), an alternative Hall thruster design offering a radical solution to efficient scaling-down and lifetime problems and concluded that its thrust performance is comparable to state-of-the-art conventional thrusters at the same power level and stable operation was observed for a wide range of operational conditions. XPT does not possess an annular discharge channel or a cylindrical one and working gas is allowed to expand into vacuum right after leaving anode. It might be considered that such a "cavity-less plasma thruster" would have very low plume divergence efficiency and mass utilization efficiency since neutral particles migrate away from the anode surface in all directions when sidewalls are absent. Therefore, farfield ion current density measurements were taken to find out plume divergence through sweeping a nude Faraday probe in the radial direction at fixed axial distances. Ion current density profiles revealed that ion beams are collimated and plumes have Gaussian distributions. The charge-weighted divergence angles were essentially similar to those of typical Hall thrusters and varied from 34 to 51 degrees. Mass utilization efficiencies ranged from 28 to 62%. Our findings question the necessity of discharge channel walls in low power Hall thrusters and provide further evidence for the usefulness of XPT for space missions. This paper also includes a description of a simple method to measure anode/wall temperature. Anode surface temperatures were measured at several operating conditions and a power law was found to describe the relation between the anode surface temperature and the discharge power.

Nomenclature

D_A	=	anode diameter	r	=	radial coordinate
I_d	=	discharge current	z	=	axial coordinate
I_b	=	beam current	$j_z(r)$	=	axial ion current density
V_d	=	discharge voltage	η_a	=	thrust/anode efficiency
V_c	=	cathode coupling voltage	η_V	=	voltage utilization efficiency
P_d	=	discharge power	η_b	=	current utilization efficiency
T	=	thrust	η_d	=	plume divergence efficiency
M_{xe}	=	equivalent mass of elemental xenon	η_m	=	mass utilization efficiency
$\dot{m}$	=	anode mass flow rate	η_q	=	charge utilization efficiency
Δ	=	discharge current oscillation amplitude	δ	=	charge-weighted divergence angle

[1] Graduate Student, Department of Space and Astronautical Sciences, burak.karadag@ac.jaxa.jp.
[2] Researcher, Institute of Aeronautical Technology, choh.shinatora@jaxa.jp.
[3] Associate Professor, Department of Space Flight System, funaki.ikkoh@jaxa.jp.

I. Introduction

HALL thrusters have high thrust density/efficiency, reliable/robust operation, simple design and extensive space flight heritage. These main features make them attractive for cube/nano/micro satellite applications. Yet, scaling-down these devices to low power levels results in short lifetime and low efficiency because thruster parts such as discharge channel wall and magnetic pole piece erode rapidly due to large surface area to volume ratio and increased plasma-wall interactions. Magnetic shielding method has been proven to lower channel wall erosion by a few orders of magnitude. Nevertheless, sputtering of iron magnetic poles was observed and this is an issue that is yet to be solved.[1] External anode layer thruster[2] and so-called wall-less Hall thruster[3] also reduces wall losses due to location of anode at channel exit but a relatively strong erosion of magnetic poles still exists. The HEMP thruster, which uses cusp magnetic structures to confine electrons, achieves nearly erosion free operation[4]. However, its thrust-to-power ratio is about half of Hall thrusters and requires high voltages for efficient operation. As a solution to this long-standing problem, we introduced external discharge plasma thruster (XPT) in our past paper[5] concluding that thrust generated by XPT is on par with conventional thrusters at the same power level (~11 mN at 250W with 25% anode efficiency without any optimization) and discharge current has SPT-level stability (Δ<0.2).

XPT achieves erosion free operation by producing and sustaining plasma discharge completely in open space. It does not have discharge channel walls, magnetic pole pieces, guard rings, magnetic core (i.e., ferromagnetic back plate) or electromagnetic coils. It operates under uncommonly high radial magnetic field strength (>1000 Gauss) with non-uniform propellant injection scheme. External discharge approach has many appealing features for space missions. Firstly, thruster head mass can be decreased one order of magnitude (e.g., $\leq$ 0.3 kg for a 300W-thruster) and very expensive/time-consuming lifetime tests would not be needed. Secondly, it can strictly reduce spacecraft contamination problems associated with thruster plume interaction. What is more, its highly simplified boundary conditions would be beneficial to plasma simulation code development.

In the classical approaches, an annular discharge channel (e.g., SPT and TAL) or a cylindrical discharge channel (e.g., end-Hall/CHT) provides long enough neutral particle residence time to ensure ionization collisions. XPT lacks any kind of discharge channel letting propellant gas to expand into vacuum at the anode exit. Therefore, it has been argued that ion beam current and plume divergence of an external discharge plasma thruster would be unfavorable since neutral gas particles are not constrained in radial direction by a cavity or sidewalls and they are free to diffuse to the vacuum in both axial and radial directions. To investigate this question, farfield ion current density measurements were taken through sweeping a nude Faraday probe in the radial direction at fixed axial distances. The measurement method was essentially the same as that used by Huang et al.[6] with some adjustments. We chose radial sweeping due to equipment constraint although it is more sensitive to non-beam ions and polar sweeps are recommended.[7] This paper presents findings from the farfield ion current density measurements of XPT with 2-mm-thick boron nitride wall (XPT-2mm).

Plasma density in a Hall thruster is directly related to residence time of neutrals in discharge channel and it is a function of anode/channel wall temperature due to rapid thermal accommodation of neutrals at anode/channel walls. Hence, knowledge of anode temperature is very valuable for accurate plasma simulations especially for an external discharge plasma thruster for which power deposition from plasma to anode is a more significant factor in the thruster operation. Yet, a direct and accurate measurement of anode temperature is a challenging task. Until now infrared cameras have been used to take thermal images of the thrusters from different observation angles at large relative distances (~2-4 m).[8,9] One of the major drawbacks using a thermal camera during the thruster operation is that its readings are questionable because the presence of plasma brings an important uncertainty in collected radiation.

This paper additionally aims to describe a method for characterizing the anode surface temperature through a commercially available low cost infrared temperature sensor. Our method differs from the preceding ones in these: 1) A viewport window or a pressurized enclosure is not needed, thus eliminating the uncertainties related to the radiation transmission, 2) Measurements are taken immediately after the thruster was turned off so, there is no disturbance due to plasma flow, and 3) The distance between the sensor and the target can be kept very short (a few cm), which greatly increases resolution and cuts out interference from other thruster surfaces. A thermocouple could also be used to measure temperature on the rear of the anode. Nevertheless, infrared sensor is able to directly measure surface temperature and does not require any structural modifications to thruster components, which can be prohibitive for a compact thruster like XPT.

II. Experimental Setup

A. Thruster and Operating Conditions

XPT is a very simple compact annular geometry low power Hall thruster. Figure 1 shows a cross section view of XPT and design details can be found elsewhere.[5] The thruster was placed in the middle of a cylindrical vacuum chamber near one end. A commercial hollow cathode was mounted at a 45° angle with respect to the thruster axis with the cathode orifice approximately 150 mm above the thruster centerline. Thruster and cathode were isolated from chamber ground. Before any data were taken, the thruster was kept in the vacuum chamber for a few hours for outgassing and then it was operated for about 1 hour to allow thruster parts to reach thermal equilibrium. During all tests cathode mass flow rate (0.29 mg/s), cathode heater current (5A), and cathode keeper current (0.3 A) were held constant. Anode potential was applied between 150 V and 250 V. Anode mass flow rate were varied between 0.48 mg/s and 1.43 mg/s with about 0.48 mg/s increments.

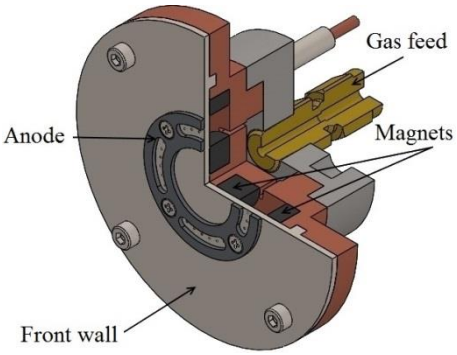

Figure 1: A cross section view of XPT. *Cathode is not shown.*

B. Vacuum Facility

All experiments were carried out in ISAS/JAXA's Space Science Chamber, which is 2.5 meters in diameter and 5 meters long. Two cryogenic pumps, one turbomolecular pump and one rotary vane pump evacuated the vacuum chamber. High purity xenon (99.995 %) was used as working gas for both the anode and the cathode. Mass flow controllers calibrated for argon was used with xenon by a conversion factor of 0.971. Background pressure was measured by a crystal ion gauge located in near upper middle of the vacuum chamber, and corrected for xenon by a coefficient given in the gauge manual. Maximum background pressure was 2.5×10^{-5} Torr at 1.43 mg/s anode mass flow rate and 0.29 mg/s cathode mass flow rate. Figure 2 shows a firing of XPT from front view.

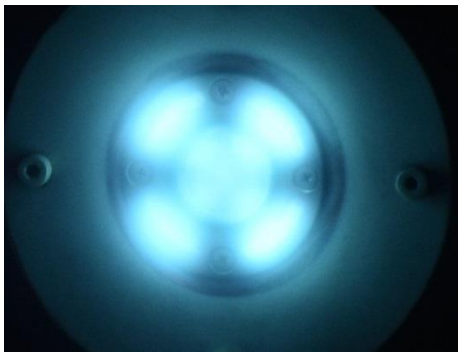

Figure 2: A front view of XPT firing.

C. Ion Current Density Measurement

1. Faraday Probe and Data Collection

Our probe design is quite similar to GRC nude Faraday probe modified by Huang et al.[6] It consists of a collector and a guard ring mounted to a macor backplate. The backplate has venting holes to reduce neutral flow effects. Both electrodes are made of 403 stainless steel and have outer diameters of 20 mm and 30 mm respectively. Gap between the electrodes is about 0.4mm wide enough to provide a flat sheath over the collector surface. The collector and the guard ring were both biased at the same potential to reduce edge effects. The probe bias voltage was varied at several radial and axial positions and it was decided that a constant bias potential of -20 V is sufficient to reach ion saturation.

The voltage across a 100 Ω current shunt resistor was recorded with a digital multimeter (Iwatsu VOAC 7523) and ion current density was calculated by dividing this voltage by the collector probe area and the shunt resistance. 2-axis motorized translation stage has a width of 108 cm providing a maximum 54 cm travel distance in +R /-R radial directions. The probe was moved along the radial direction with 20 mm resolution starting at +R and stopped at each point about 3 seconds to measure the shunt voltage. Moving the probe from +R to –R took approximately 3 minutes. The thruster plume was also scanned in the opposite direction to check repeatability. Measurements were taken at two fixed axial distances 4 and 8 D_A (anode diameter). Figure 3 shows the translation stage, probe design and electrical diagram for data collection.

Vertical aluminum arm carrying the probe head was covered with Kapton. Twisted shielded pair cables were used and the shield was grounded to the vacuum chamber walls for signal noise reduction. Discharge currents were not disturbed during the probe sweeps. Practices recommended by Brown et al.[7] were generally adopted.

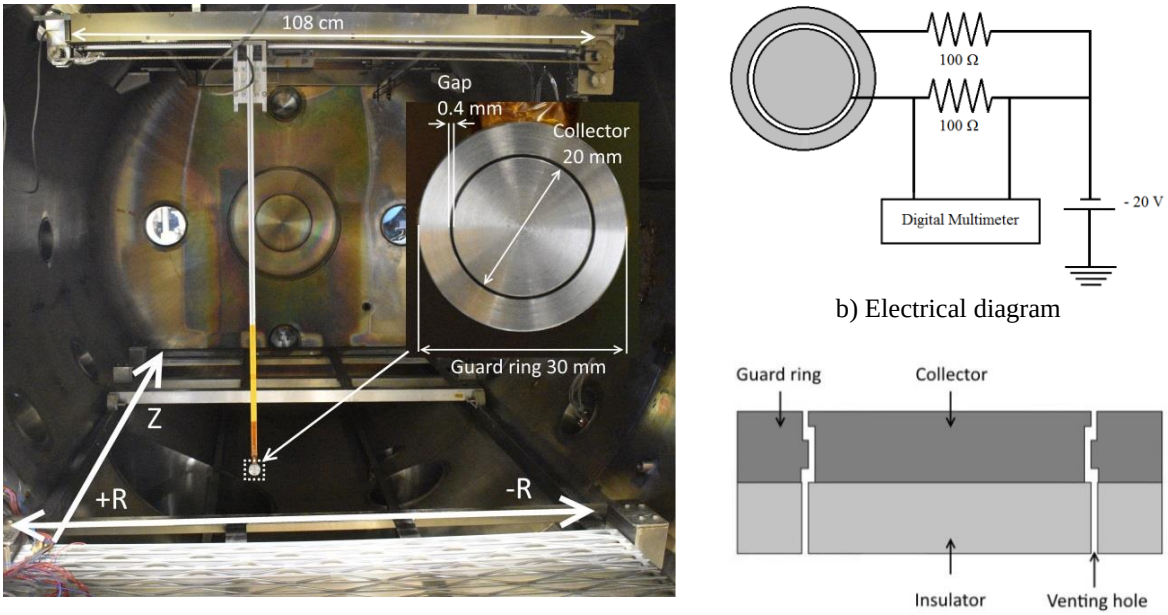

a) Translation stage and the probe

b) Electrical diagram

c) Probe cross section

Figure 3: Probe design and data collection.

2. Data Processing

For ion current density measurements in a cylindrical coordinate system, Faraday probe collects axial component of the local ion current density. Assuming the plume has symmetry about the z-axis, total ion beam current I_b and the charge-weighted divergence angle δ are approximated as below:

$$I_b = 2\pi \int_0^\infty j(r) r dr \tag{1}$$

$$< \cos\delta >_j = \frac{2\pi \int_0^\infty j_z(r) \cos\theta r dr}{2\pi \int_0^\infty j_z(r) r dr}, \cos\theta = \frac{z}{\sqrt{r^2 + z}} \tag{2}$$

where z is the distance between thruster exit and probe face and $j_z(r)$ is local ion current density measured at each radial coordinate r.[6] Equation (1) and Eq. (2) dictate that probe should be swept from the center of thruster exit plane to infinity in the radial direction. However, this is not feasible due to the finite width of the translation stage or vacuum chamber. We chose half-width of the translation stage as the integration limit because calculated total ion beam current to discharge current ratios (≥0.54 and ≤ 0.82) were reasonable for all the operating conditions.

3. Efficiency Analysis

Anode efficiency η_a is the indicator of overall energy conversion of the thruster-head. To analyze thrust generation processes it can be divided into voltage utilization efficiency η_V, current utilization efficiency η_b, charge utilization efficiency η_q, mass utilization efficiency η_m, and plume divergence efficiency η_d which is also called beam utilization efficiency as:

$$\eta_a = \frac{T^2}{2\dot{m} I_d V_d} = \eta_V \eta_b \eta_q \eta_m \eta_d \tag{3}$$

where T is thrust, ṁ is anode mass flow rate, I_d is discharge current, and V_d is anode potential. The voltage utilization efficiency explains amount of the potential energy which is converted to kinetic energy and defined as the ratio of beam voltage to discharge voltage ($\eta_V = V_b/V_d$). The beam voltage can be assumed to be $V_b = V_d - V_L$, where V_L is the loss voltage. The assumed value of V_L was 15 V. Then η_V can be estimated as:

$$\eta_V = 1 - \frac{V_L}{V_d} \tag{4}$$

The charge utilization efficiency measures overall charge state of the beam ions and decreases linearly with applied anode potential. Its value can be assumed to equal to 0.99 for Hall thrusters operating at low anode potentials (< 300 V). The current utilization efficiency compares thrust-generating ion current to discharge and beam utilization efficiency is useful to analyze plume focusing. They are calculated using the equations shown below:

$$\eta_b = \frac{I_b}{I_d} \tag{5}$$

$$\eta_d = \left(< \cos\delta >_j\right)^2 \tag{6}$$

Finally mass utilization efficiency can be estimated through the measured thrust as:

$$\eta_m = \frac{T}{\dot{m}\sqrt{\frac{2e(V_d - V_L)}{M_{xe}}}} \tag{7}$$

where e is the elementary charge and M_{xe} is the equivalent mass of elemental xenon. Details of this efficiency breakdown scheme can be found elsewhere. [6, 10]

4. Uncertainty Analysis

The digital multimeter has an input resistance of 1000MΩ yielding to ~20 nA probe leakage current for a bias of -20 V. Secondary electron emission from the collector due to impingement of ions with energies lower than 300 eV can be assumed to be insignificant for stainless steel surfaces.[11] Tungsten coating might be necessary at discharge potentials over 300V. Positioning error of the translation stage is of ±1 mm. Systematic errors associated with Bohm current collection, sheath expansion, divergence angle reference point and thermionic emission due to excessive probe heating can be disregarded for the far-field ion current density measurements. Random errors and digital multimeter measurement error (e.g. drift, offset, noise, and etc.) were estimated to be ±0.05 mA/cm^2 by comparing consecutive measurements.

The effective collection area and background pressure effects can be given as two main sources of uncertainty. The collector and the guard ring have the shape of a cylinder with flat and curved surfaces. Ions entering the gap between the collector and guard ring are collected at the curved surfaces and give rise to uncertainty in the effective collection area. The area correction factor suggested by Brown[7] is not suitable for correcting radially swept data since the probe face does not remain constantly pointed at the thruster as in a polarly swept probe. It was still calculated and found to be 4% for our probe corresponding to an uncertainty of -4 % in ion current density. Quantifying background pressure effects (i.e. CEX collisions and neutral ingestion) is also difficult for the radially swept probe because the distance between the probe and the thruster is not constant. All things considered, it seems reasonable to assume a conservative range of ±10 % for the total uncertainty. Measurements should be repeated at a minimum of three different background pressures for extrapolation of ion current density to zero. This was avoided because polar sweeps are more advisable for the space environment predictions, which is beyond the scope of this paper.

D. Anode Temperature Measurement

1. Data Collection

We employed a Calex PyroUSB CF, which was kindly provided by GMI Japan K.K., to collect infrared energy of the anode. The sensor can measure temperatures up to 1000 °C and its minimum focal spot size is 5 mm (i.e., it reads average temperature of a spot 5 mm in diameter) at 100 mm distance. The sensor was mounted on the translation stage inside the vacuum chamber and connected to PC through USB port. The output signal was processed and recorded using specialized software supplied by the manufacturer. The thruster was fired at operating conditions of 200-250 V and 0.95-1.43 mg/s mass flow rates. At each condition, the anode was allowed to reach thermal equilibrium by continuous operation for 30 minutes.

During firings, the sensor was put in a rest position behind the thruster and then moved to the front of the anode right after the thruster shut down. Moving the sensor from its rest position to the front of the anode took four

seconds. Temperature was measured at one point on the anode centerline, which is the closest to the cathode and marked by the red dot laser seen in Fig. 4 (a). The ambient temperature near the thruster was also measured by a thermocouple.

2. Determining Anode Emissivity and Data Processing

Every grey body hotter than absolute zero emits light at infrared spectrum or infrared radiation whose intensity is proportional to the to the fourth power of its absolute temperature and emissivity ($E= \sigma\varepsilon T4$). Non-contact temperature sensors detect intensity of this infrared radiation and convert it into a temperature value using a pre-defined emissivity coefficient. Emissivity significantly depends on chemical composition, surface characteristics such as temperature, wavelength and observation direction.

The anode of XPT is made of 1 mm-thick molybdenum. Molybdenum is normally a silvery-white metal and has an emissivity between 0.05-0.2. Over the past experiments, a black material has been deposited on the anode and its surroundings as seen in Fig. 4(a). This black material is electrically conducting and it originates from the beam damper and the vacuum chamber walls sputtered away as ions impinge. Ceramic bolts, one of which is marked with dashed blue circle were replaced with brand-new ones for color comparison. Material deposition on both the anode and the front wall constitutes a visual evidence for erosion free operation.

To find emissivity of the deposited material, the anode was heated by a coil wrapped around the thruster body and its temperature was measured under vacuum condition by the infrared (IR) sensor and a thermocouple. A second thermocouple was placed near the anode for ambient temperature compensation. The sensor's emissivity setting was adjusted until it displays the temperature of the thermocouple. Fig. 4(b) shows the emissivity measurement setup and Fig. 5(a) compares the thermocouple and infrared sensor readings. The emissivity of the material deposited on the anode was 0.83 ± 0.01. Note that the thermocouple and the infrared sensor measures different points but the anode can be expected to have a uniform temperature distribution due to the symmetric structure of the heater coil and the thruster.

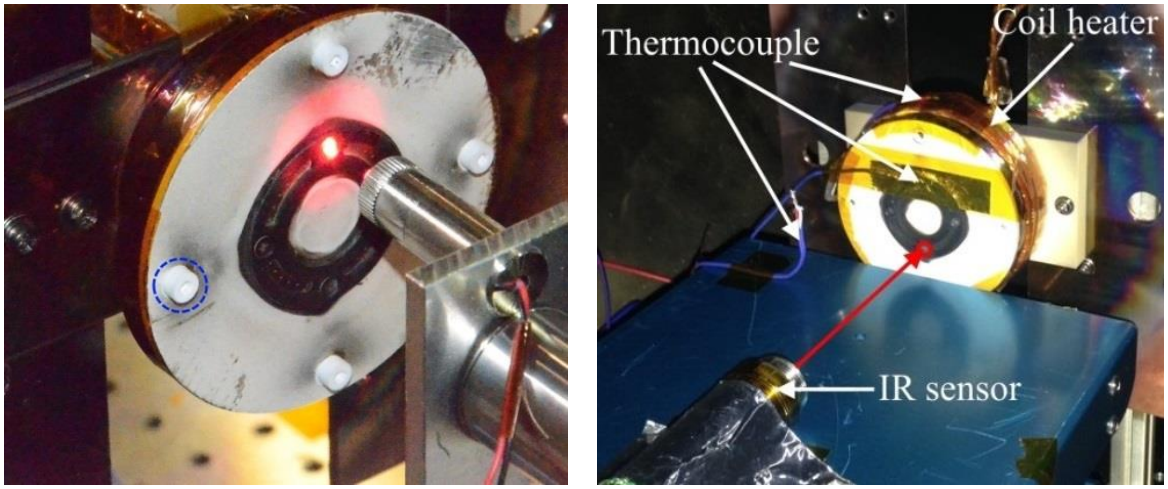

a) Sensor positioning b) Emissivity measurement setup

Figure 4: Sensor positioning and emissivity measurement setup.

The temperature at t = 0 s was extrapolated from the cool-down curves of the anode, which was captured for three minutes. Figure 5(b) shows a cool-down curve sample and exponential fit coefficients calculated by Origin data analysis software. The exponential fits were of the form:

$$y = A_1 \exp\left(\frac{x}{c_1}\right) + A_2 \exp\left(\frac{x}{c_2}\right) + A_3 \exp\left(\frac{x}{c_3}\right) + y_0 \quad (8)$$

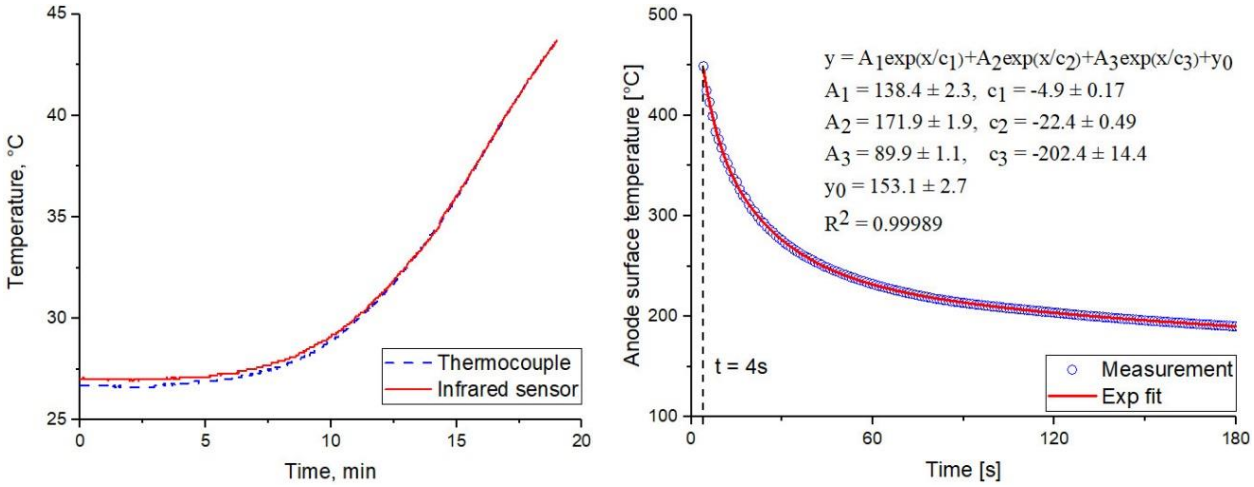

a) Comparison of thermocouple and infrared sensor b) Cool-down curve for 250V 1.43 mg/s

Figure 5: IR sensor calibration and a cool-down curve of the anode.

3. Uncertainty Analysis

Emissivity is the prevalent source of uncertainty. As stated before, chemical composition, surface characteristics, wavelength and observation angle are all the factors affecting emissivity. Emissivity is nearly constant when the sensor line of sight is normal to the anode surface. Spectral range of infrared sensors is from 7 to 14 μm and metals have relatively uniform emissivity at this wavelength range. Changes in chemical composition and surface characteristics of the anode except the surface temperature are expected to be insignificant. However, as surface temperature increases, emissivity of metals will also increase. Unfortunately, we were not able measure the anode emissivity at temperatures over 45 °C because of a coil failure. So it is hard to estimate the uncertainty in emissivity without experiment but we note here that actual anode temperatures should be underestimated. Regarding instrument uncertainty, infrared sensor has ±1% reading accuracy and thermocouple thermometer is able to measure temperature to 0.1°C accuracy.

In addition, although the regression lines almost perfectly fitted the data, travel time of the sensor from its rest position the anode downstream is considered to be long. The anode temperature would decrease sharply in the first four seconds which increases the uncertainty resulting from the extrapolation. It is therefore recommended that the sensor travel time should be reduced down to 1s or lower by using high speed translation stages. Also, it would be favorable to install an aperture stop on the infrared sensor head not to allow any material deposition on the sensor lens.

III. Results and Discussion

E. Ion Current Density Profile

The ion current density profiles measured at axial distances of 4-8 D_A are given in Fig. 6. We can see that the current density profiles are symmetric with respect to the thruster centerline even though XPT has a non-uniform neutral injection scheme dividing plasma flow into four regions as shown in Fig. 2. The plume becomes more diffuse and the peak current density decreases with axial distance due to particle scattering from the centerline to the plume wings. When the anode potential increased to 250V the peak current density also increases due to further ionization.

High ion current density region called the “center spike” is observed on thruster centerline. Double hump peaks that are often seen in Hall thruster plume profiles due to the annular discharge channel were not observed. This may be due to large size of the collector surface area decreasing the sweep resolution. The ion current densities should be overestimated due to ionization and charge exchange collisions of background neutral particles. However, radially swept probe data confirms that the far-field plume is strongly Gaussian and ion beam is well focused.

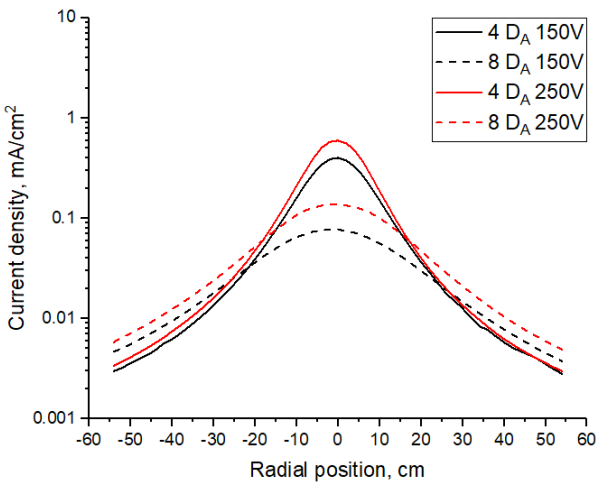

a) Ion current density profile 0.48 mg/s

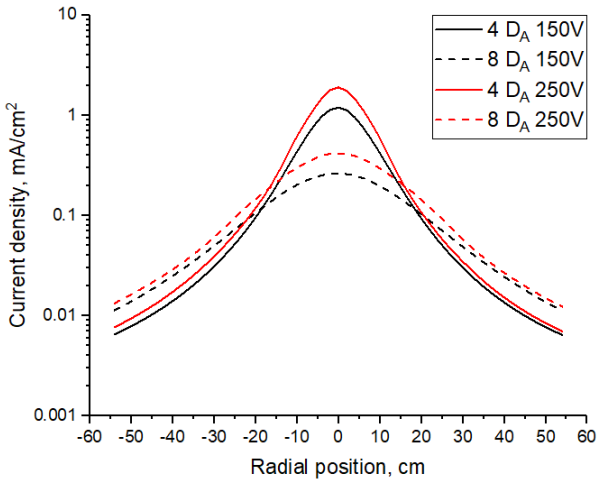

b) Ion current density profile 0.95 mg/s

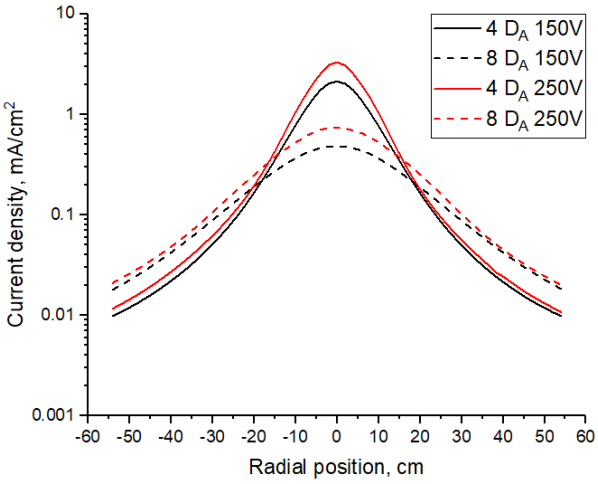

c) Ion current density profile 1.43 mg/s

Figure 6: Ion current density profiles plotted on logarithmic scale. *D_A means anode diameter.*

F. Anode Surface Temperature

Thermal simulations are commonly performed to estimate anode temperature but anode temperature should be known accurately for meaningful comparisons between experiments and simulations because discharge current is a strong function of anode temperature especially in case of XPT. For instance, we observed about 7% decrease (from 1.01A to 0.94 A at 250 V-0.98 mg/s) in discharge current from beginning of the thruster firing until the anode reached the thermal equilibrium.

Anode surface temperatures for different operating conditions are given in Fig. 7. It turns out that XPT has the same level of anode temperature as in high power Hall thrusters. This can be attributed to its small anode thickness (1mm) and poor thermal conductivity due to ceramic front wall.

A previous work using infrared imaging showed that there is a relation between discharge channel wall temperature and discharge power and it can be expressed according to the following formula: $T = a + b \times P_d{}^n$ where a is wall temperature before thruster firing, b and n are parameters depending on wall geometry and/or material.[8] We found that the same power law can be used to express the relation between anode surface temperature and discharge power. Anode surface temperatures rises with discharge power according to the following equation: $T = 300 + (33.2 \pm 5.8) \times P_d{}^{(0.46 \pm 0.03)}$, which fits the data with an R^2 value of 0.9988. This equation will be used as a reference in our future numerical study of XPT.

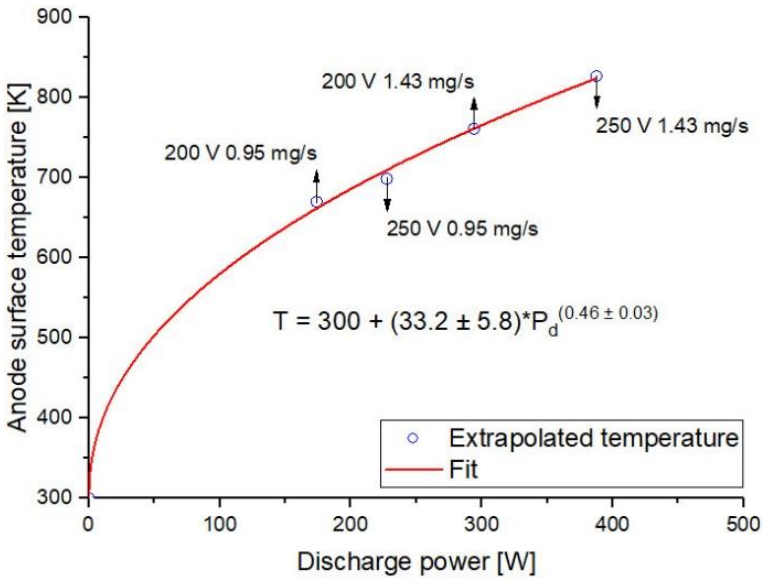

Figure 7: Anode surface temperature against discharge power.

G. Efficiency Breakdown

Table 1 shows integrated ion beam currents, efficiency breakdown and plume divergence half-angles calculated for the ion current densities. The mass utilization efficiency and plume divergence efficiency seems to be the dominant loss mechanisms. Mass utilization efficiency indicates to what extent neutral propellant gets ionized and contributes to thrust. It increases proportionally to mass flow rate and discharge voltage since increasing mass flow rate results in higher neutral densities and decreased ionization mean free path. A higher discharge voltage produces more ions due to increased electron density and temperature and improves current utilization efficiency.

Efficiency components for 0 D_A were estimated through extrapolation of the ion current densities measured at 4 and 8 D_A. This was done because such estimation at the thruster exit corrects errors related to charge exchange collisions and the integration limit in Eq. (1). It may be thought that linear extrapolation with two points is subject to great uncertainty, but extrapolation with three points yielded only 1.3% difference in the estimated beam current for 250 V 1.43 mg/s operating condition. So linearity assumption can be made. Note that there is still error arising from ionization of the background neutrals. Besides, E × B probe measurements are not available but we can say that fraction of multiply charged ions should be large for some operating conditions because estimated beam currents exceeds the theoretical limit for a beam composed exclusively of singly charged ions.

Anode efficiencies determined by probe data matches well with those calculated directly from thrust stand results. Even though the peak current density decreases and the plume becomes more diffuse, plume divergence efficiency increases with axial distance of the probe because the integration area arising from Eq. (1) increases linearly from the thruster center to the radial axis limit.

Standard high power Hall thrusters can achieve mass, plume divergence and discharge current utilization efficiencies of 80-90%, 70-90%, and 70-80% respectively at their optimum operating conditions.[12, 13] Current utilization efficiency is the dominant factor that limits the thrust efficiency and the efficiency loss can get severe for low power Hall thrusters. XPT achieves relatively moderate mass utilization efficiency and plume divergence efficiency while its estimated current utilization efficiency varies between 80-100%. This result is significant considering that neutrals and magnetized plasma discharge are not confined to an annular or cylindrical cavity. It demonstrates that external discharge approach is effective in improving current utilization efficiency as power deposition on the discharge channel walls is mostly eliminated.

Table 1. Efficiency Breakdown

$\dot{m}$ [mg/s]		V_d [V]	D_A	I_d	I_b	η_V	η_b	η_m	η_d	η_q	δ [°]	η_a^F	η_a^T
0.48	Est →	150	0	0.29	0.29	0.90	1.00	0.28	0.43	0.99	49.1	0.11	0.09
		150	4	0.29	0.22	0.90	0.76	0.28	0.46	0.99	47.5	0.09	0.09
		150	8	0.29	0.15	0.90	0.59	0.28	0.56	0.99	41.6	0.08	0.09
	Est →	250	0	0.35	0.33	0.94	0.94	0.32	0.40	0.99	50.5	0.11	0.10
		250	4	0.35	0.28	0.94	0.79	0.32	0.48	0.99	46.0	0.11	0.10
		250	8	0.35	0.23	0.94	0.65	0.32	0.58	0.99	40.2	0.11	0.10
0.95	Est →	150	0	0.86	0.69	0.90	0.80	0.39	0.41	0.99	50.4	0.11	0.11
		150	4	0.86	0.58	0.90	0.67	0.39	0.48	0.99	46.1	0.11	0.11
		150	8	0.86	0.47	0.90	0.54	0.39	0.57	0.99	40.8	0.11	0.11
	Est →	250	0	0.94	0.91	0.94	0.97	0.54	0.46	0.99	47.1	0.22	0.20
		250	4	0.94	0.77	0.94	0.82	0.54	0.51	0.99	44.4	0.21	0.20
		250	8	0.94	0.63	0.94	0.67	0.54	0.60	0.99	39.2	0.20	0.20
1.43	Est →	150	0	1.53	1.20	0.90	0.78	0.50	0.42	0.99	49.5	0.15	0.15
		150	4	1.53	1.02	0.90	0.66	0.50	0.49	0.99	45.4	0.15	0.15
		150	8	1.53	0.84	0.90	0.54	0.50	0.58	0.99	40.3	0.14	0.15
	Est →	250	0	1.64	1.52	0.94	0.93	0.62	0.48	0.99	46.3	0.26	0.23
		250	4	1.64	1.31	0.94	0.80	0.62	0.52	0.99	43.9	0.24	0.23
		250	8	1.64	1.08	0.94	0.66	0.62	0.61	0.99	38.9	0.23	0.23
		250	12	1.64	0.88	0.94	0.54	0.62	0.68	0.99	34.2	0.21	0.23

Est shows values at 0 D_A estimated using a linear extrapolation.
η_a^F is anode efficiency based on the Faraday probe data, $\eta_a^F = \eta_V\eta_b\eta_q\eta_m\eta_d$.
η_a^T is anode efficiency derived from thrust stand data, $\eta_a^T = T^2/(\dot{m}P_d)$.
η_q was assumed 0.99.

Excessive anode temperature may be responsible for the moderate mass utilization efficiency as it decreases residence time of neutrals and enable them to escape without getting ionized. Anode temperature can be decreased by modifying the anode design (e.g. extending its rear surface inside the thruster body to increase the thickness) and heat conduction path. The current magnetic circuit design of XPT provides poor radial magnetic field homogeneity. A better plume divergence efficiency can be achieved by optimizing the magnetic field topography.

IV. Conclusion

The plume of external discharge plasma thruster (XPT) was characterized by radially sweeping a nude Faraday probe. The charge-weighted divergence angles and mass utilization efficiencies varied from 34 to 51 degrees and 28 to 62% respectively. It was uncovered that ion beam profiles are Gaussian and symmetric with respect to the thruster centerline despite the azimuthally non-uniform plasma. These experimental results support our previous hypothesis[14] that external discharge plasma thruster can achieve propellant utilization efficiency and plume divergence efficiency as much as conventional Hall thrusters in low power range. Additionally, an alternative method was presented for measuring anode/wall surface temperature of electric thrusters.

Acknowledgments

B. Karadag thanks Japanese Ministry of Education, Culture, Sports, Science, and Technology (MEXT) for his scholarship. Authors thank Assistant Prof. Watanabe Hiroki for his helpful discussion. This study was supported by ISAS/JAXA as a collaborative program with the Space Chamber Laboratory.

References

[1]Jorns, B. A., Dodson, C., Anderson, J., Goebel, D. M., Hofer, R. R., Sekerak, M., Ortega, A. L., and Mikellides, I., "Mechanisms for pole piece erosion in a 6 kw magnetically-shielded Hall thruster," *52nd AIAA/SAE/ASEE Joint Propulsion Conference*, Salt Lake City, Utah, 2016, AIAA 2016-4839.

[2]Semenkin, A. V., "Investigation of erosion in anode layer thruster and elaboration high life design scheme," *23th International Electric Propulsion Conference*, Seattle, 1993, IEPC-93-231.

[3]Mazouffre, S., Tsikata, S., and Vaudolon, J., "Development and experimental characterization of a wall-less Hall thruster," *Journal of Applied Physics 116*, 243302 (2014).

[4]Koch, N., Harmann, H. P., and Kornfeld, G., "Development and Test Status of the Thales High Efficiency Multistage Plasma (HEMP) Thruster Family," *29th International Electric Propulsion Conference*, Princeton, 2005, IEPC-2005-297.

[5]Karadag, B., Cho, S., Oshio, Y., Funaki, I., and Komurasaki, K., "Preliminary Investigation of an External Discharge Plasma Thruster," *52nd AIAA/ASME/SAE/ASEE Joint Propulsion Conference & Exhibit*, Salt Lake City, Utah, 2016, AIAA 2016-4951.

[6]Huang, W., Kamhawi, H., and Shastry, R. "Farfield Ion Current Density Measurements before and after the NASA HiVHAc EDU2 Vibration Test," *48th AIAA/ASME/SAE/ASEE Joint Propulsion Conference & Exhibit*, Atlanta, Georgia, 2012, AIAA 2012-4195.

[7]Brown, D. L., Walker, M. L. R., Szabo, J., Huang, W., and Foster, J. E., "Recommended Practice for Use of Faraday Probes in Electric Propulsion Testing," *Journal of Propulsion and Power*, Vol. 33, No. 3, 2017, pp. 582-613.

[8]Mazouffre, S., Echegut, P., and Dudeck, A., "A calibrated infrared imaging study on the steady state thermal behaviour of hall effect thrusters," *Plasma Sources Science and Technology*, Vol. 16, No. 1, 2007, pp. 13-22.

[9]Spektor, R., Beiting, E. J., et al., "Infrared Thermographic Diagnostic for Imaging Hall Thrusters," *33rd International Electric Propulsion Conference*, Washington, 2013, IEPC-2013-452.

[10]Brown, D. L., Larson, C. W., Beal, B. E., and Gallimore, A. D., "Methodology and Historical Perspective of a Hall Thruster Efficiency Analysis," *Journal of Propulsion and Power*, Vol. 25, No. 6, 2009, pp. 1163-1177.

[11]Azziz, Y., "Experimental and Theoretical Characterization of a Hall Thruster Plume," PhD Thesis, Massachusetts Institute of Technology, Boston, 2007.

[12]Hofer, R. R., and Gallimore, A. D., "Efficiency Analysis of a High-Specific Impulse Hall Thruster," *40th AIAA/ASME/SAE/ASEE Joint Propulsion Conference & Exhibit*, Ft. Lauderdale, Florida, 2004, AIAA-2004-3602.

[13]J. L. Ross, "Probe studies of a Hall thruster at low voltages," Ph.D. Dissertation, Michigan Technological University, Houghton , 2011.

[14]Karadag, B., Cho, S., and Funaki, I., "Numerical Investigation of an External Discharge Hall Thruster Design Utilizing Plasma-lens Magnetic Field," *Space Transportation Symposium FY2015*, Sagamihara, Kanagawa, 2015, STEP-2014-032.